Leading-edge tubercles delay stall on humpback whale (*Megaptera novaeangliae*) flippers

D. S. Miklosovic
Aerospace Engineering Department, United States Naval Academy, Annapolis, Maryland 21402

M. M. Murray
Mechanical Engineering Department, United States Naval Academy, Annapolis, Maryland 21402

L. E. Howle[a)]
Mechanical Engineering and Materials Science Department and Center for Nonlinear and Complex Systems, Duke University, Durham, North Carolina 27708-0300

F. E. Fish
Department of Biology, West Chester University, West Chester, Pennsylvania 19383

(Received 11 December 2003; accepted 2 February 2004; published online 15 March 2004)

The humpback whale (*Megaptera novaeangliae*) is exceptional among the baleen whales in its ability to undertake acrobatic underwater maneuvers to catch prey. In order to execute these banking and turning maneuvers, humpback whales utilize extremely mobile flippers. The humpback whale flipper is unique because of the presence of large protuberances or tubercles located on the leading edge which gives this surface a scalloped appearance. We show, through wind tunnel measurements, that the addition of leading-edge tubercles to a scale model of an idealized humpback whale flipper delays the stall angle by approximately 40%, while increasing lift and decreasing drag. © *2004 American Institute of Physics.* [DOI: 10.1063/1.1688341]

The turning performance of aquatic animals is constrained by morphology with the mobility and flexibility of the body and the hydrodynamic characteristics and position of the control surfaces influencing the animal's turning performance. The baleen whales of the cetacean suborder Mysticete are the largest of all animals. Much of the body is inflexible because of their specialized feeding system, which restricts their maneuverability. However, the humpback whale (*Megaptera novaeangliae*) is unusual compared to other mysticetes in its ability to undertake acrobatic turning maneuvers in order to catch prey.[1,2] Humpback whales utilize extremely mobile, high-aspect-ratio flippers for banking and turning. Large rounded tubercles, shown in the photographs of Fig. 1, along the leading edge of the flipper are morphological structures that are unique in this animal. The position, size and number of tubercles on the flipper suggest analogs with specialized leading-edge control devices associated with improvements in hydrodynamic performance on biological[3] and engineered[4] lifting surfaces. It has been hypothesized that these leading-edge tubercles can modify the hydrodynamic characteristics of the flipper to increase its effectiveness in turning.[5,6] In this study, we report wind tunnel measurements of the lift and drag, along with other parameters, as a function of the angle of attack of idealized scale models of a humpback whale flipper with and without tubercles.

We constructed two scale models of a humpback pectoral flipper; one with and one without leading-edge tubercles. We show both of these models in Fig. 2. The flipper planform geometry was modeled, roughly, after the left pectoral flipper of a 9.02 m male humpback whale.[6] Photographs of whale flippers reveal variability in the size and shape of the tubercles among individuals. Therefore, we did not intend, here, to model a specific flipper but rather capture the gross morphology that is common to the species. We do expect that the details of the geometry (for example, abrupt changes in surface curvature) would influence the performance of an individual flipper. Our first (smooth) model flipper had a smooth leading edge with a shape that closely matched the average leading-edge geometry of the animal while our second (scalloped) flipper had a sinusoidal leading-edge profile approximating the pattern found on the specimen flipper. Consistent with the animal, the sinusoidal pattern had both an intertubercle spacing and a tubercle amplitude that decreased with spanwise (distal) location. The flipper cross-sectional profile is similar to conventional turbulent-flow airfoils with a maximal thickness of approximately 20%.[6] Therefore, we constructed our models based on a symmetrical NACA 0020 foil section. Both model flippers, machined on a CNC mill from 3.81 cm thick clear polycarbonate, had a maximal chord of 16.19 cm and a span of 56.52 cm. The surface was coated with self-leveling epoxy (West Systems). After curing, the surfaces were wet sanded with progressively finer emery paper down to 600 grit.

Our tests were performed in the low speed closed-circuit wind tunnel at the United States Naval Academy. The tests were conducted at incompressible flow conditions, with the aerodynamics simulating the hydrodynamics of flow around the flipper. As the flippers are not oscillated during turning

a)Author to whom correspondence should be addressed; electronic mail: laurens.howle@duke.edu

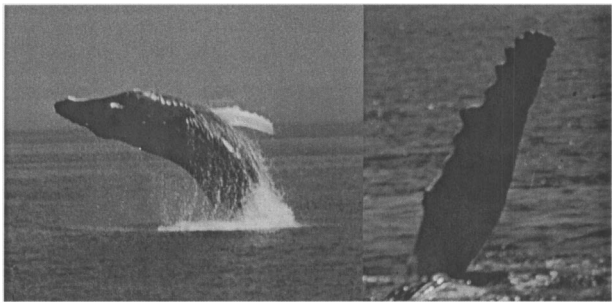

FIG. 1. Left: photograph of a breaching humpback whale (*Megaptera novaeangliae*) showing the size of the pectoral flippers relative to the animal. Right: detail view of a pectoral flipper. This flipper shows the characteristic tubercles giving the leading edge a scalloped shape. The trailing edge is relatively free from these morphological complexities. Photographs: Dennis Bowen.

maneuvers by the whale, we were justified in considering only steady state flow conditions in testing. The maximum Mach number reached during our tests was 0.2. The vented test section has a cross section of 54×38 in. (137×97 cm) and a length of 94 in. (239 cm). A contraction ratio of 6.23

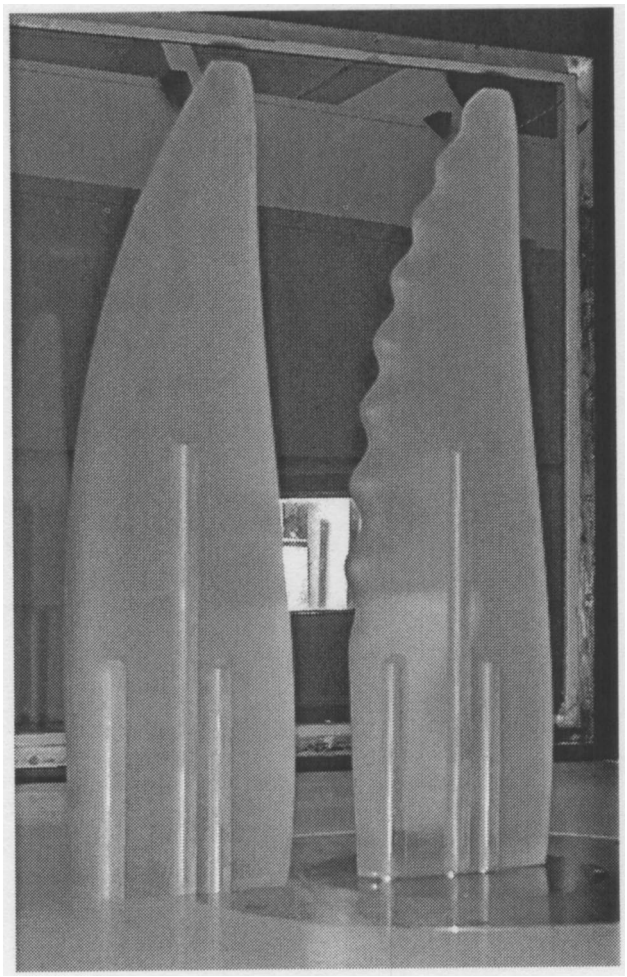

FIG. 2. Smooth (left) and scalloped (right) idealized humpback whale flipper models used for wind tunnel testing of lift, drag, efficiency, and stall behavior. While testing, only one of the models is mounted in the wind tunnel. These idealized, scale models, milled from clear polycarbonate sheet, use a NACA 0020 sectional profile (20% thick).

enhances production of a uniform flowfield, as does a quadruple screen configuration in the upstream settling chamber. The wind tunnel experiments were conducted at uncorrected Reynolds numbers ($\mathrm{Re}\equiv\overline{c}U_\infty\nu^{-1}$) in the range $5.05\times10^5-5.20\times10^5$ as referenced to the freestream velocity, U_∞, mean chord, $\overline{c}$, and the kinematic viscosity of the air, ν. For the whale, we would expect the Reynolds number to be in the neighborhood of $\mathrm{Re}\approx10^6$ based on a flipper mean chord of 50.7 cm[6], a lunge-feeding speed of 2.6 ms^{-1} and seawater viscosity of $\nu=1.35\times10^{-2}$ $\mathrm{cm}^2\,\mathrm{s}^{-1}$. Although the Reynolds number used in our experiments is approximately half of that estimated for the animal, it is well within the operating range of adult animals and perhaps close to the maximum for young animals. Nevertheless, we performed tests on the effect of the Reynolds number on the measured quantities and found that for $\mathrm{Re}>4\times10^5$, the lift coefficient was relatively insensitive to Re at moderate incidence angles.

Each flipper model was mounted vertically in the wind tunnel on a rotating yaw table which changed the local pitch angle. The models were rotated through an angle of attack, α, range of $-2°$ to $+20°$ ($\Delta\alpha=0.5°$) using a pitch–pause technique. This included some hysteresis tests that involved first increasing the angle of attack from $-2°$ to $+20°$, and then decreasing the angle of attack from $+20°$ to $-2°$.

Aerodynamic forces and moments were transmitted to a six-component Schenck external compact platform balance located beneath the test section yaw table. The standard deviation in force measurement over a representative 15-minute test at a constant flow condition has been demonstrated to be ±0.03 lb (0.13 N) in drag, ±0.24 lb (1.08 N) in lift, and ±0.08 ft-lb (0.11 Nm) in pitching moment. The coefficients for these forces have standard deviations of ±0.0003, ±0.003, and ±0.001, respectively, for the present wind tunnel models. Additionally, the test section was instrumented with pressure transducers and a thermocouple to obtain real-time measurement of freestream velocity and air density.

The millivolt-level balance output signals were monitored and acquired using a $6\frac{1}{2}$-digit Agilent 34970A data acquisition/switch unit with a 34901A multiplexer module. Serial connections to a Jetter Mikro PLC were accessed for monitoring the model orientation encoders. A conventional HP-IB (IEEE 488.2) communications link interfaced the data acquisition unit with the host laptop computer. Scan rates as high as 250 channels per second were executed with this system.

During data acquisition, nine channels were scanned (six balance outputs including three force measurements and three moment measurements, the balance excitation voltage, the test section dynamic pressure, and the freestream air temperature). A single scan was taken at $6\frac{1}{2}$-digit precision over an integration aperture of 20 power line cycles, as prescribed for high common mode rejection on low-level signals. The effective scan rate was 0.6 channels/s. Approximately 5 s were allocated for tunnel transients to diminish prior to triggering the data acquisition system. Each data acquisition scan process required about 6 s to complete. Further details of the measurement system are available elsewhere.[7]

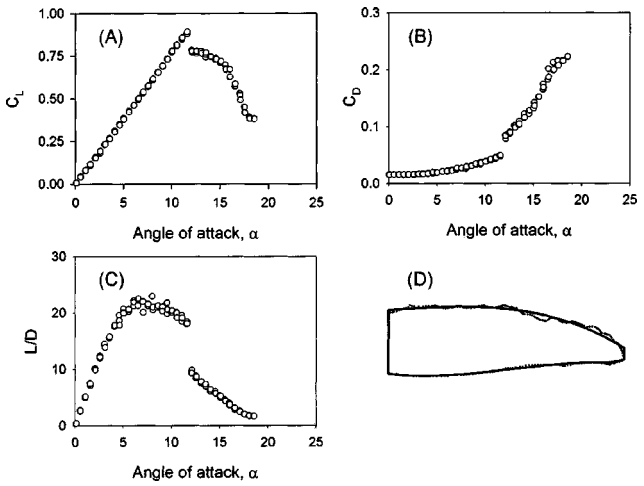

FIG. 3. Lift and drag data for the smooth whale flipper model. (a) Wind tunnel measurement of the lift coefficient, C_L, shown as a function of the angle of attack, α. (b) Drag coefficient, C_D, shown as a function of the angle of attack. (c) Aerodynamic efficiency, L/D, which quantifies the drag cost of producing lift, shown as a function of the angle of attack. (d) Planform profile of the smooth flipper model (solid line) superimposed on the actual flipper profile (dotted line). In this orientation, flow would progress from top to bottom. (a) and (b) show that stall occurs near $\alpha \approx \pm 12°$.

The primary nondimensional parameters describing the aerodynamic forces placed on the models by the flow are the drag coefficient, $C_D \equiv 2D(\rho U_\infty^2 A)^{-1}$, and the lift coefficient, $C_L \equiv 2L(\rho U_\infty^2 A)^{-1}$. While we also measured the side force and the three moment coefficients, we do not report these here. In the expressions for the drag and lift coefficients, D and L are, respectively, the drag force and the lift force, and ρ is the air density. The values of the projected planform area, A, and the mean chord, $\overline{c}$, for both the smooth and scalloped models are 737.7 cm^2 and 13.04 cm.

Reynolds number sensitivity was established using the smooth flipper model. With the Reynolds number varied from 135 000 to 550 000, the lift and drag coefficients were measured at angles of attack of 0° and 5°. Although both the lift and drag coefficients show a notable dependence at the lower Reynolds numbers, the curves flatten out to indicate very little or no Reynolds number dependence at the test conditions of the present study. The lift coefficient is the most insensitive, with essentially no dependence for Reynolds numbers above 200 000. The drag coefficient approaches a constant value for our test angles of attack above Reynolds numbers of approximately 400 000, although a truly constant trend is not established. We expected that, because of the narrow tip, the stall behavior on the outboard portion of the flipper would be strongly dependent on the Reynolds number, especially at the lower range. Nevertheless, the C_D values decrease at such a low rate at the upper range of the Reynolds number sweep, particularly for $\alpha = 5°$, that the Reynolds sensitivity can be assumed to be negligibly small.

The lift curve for the smooth model, Fig. 3(a), shows a linear relation between the lift coefficient, C_L, and the angle of attack, α, for angles below 12°. In this region, the slope of the lift curve has the value $a \equiv dC_L/d\alpha = 0.0769\ \text{deg}^{-1}$. This measured slope is within 5% of the results calculated from thin airfoil theory[8] (based on an effective aspect ratio of 8.7). The constant-slope segment of the lift curve indicates that the flow is attached to the surface of the model flipper and stall is absent during this flow state.

The onset of stall occurs suddenly but the loss in lift is not as considerable as we would expect with complete leading-edge flow separation. For the smooth flipper model, α_{stall} occurs at 12°, yet the drop in C_L is only 13%. This small loss in lift might be due to flow separation near the distal region before flow separation near the proximal region resulting in only a partial loss of lift. While we did not perform flow visualization to validate this hypothesis, the high taper of the outboard portion of the flipper suggests that low Reynolds number effects are present here that might not be present at inboard stations. These low Reynolds number effects could result in partial stall at the distal end of the flipper. The subsequent decrease in C_L from 0.78 to 0.38 reveals a progression of stall as we increase α from 12.1° to 18.5°.

The drag coefficient, C_D [Fig. 3(b)], shows that the onset of stall occurs with an increase in drag from $C_D = 0.0485$ to $C_D = 0.0821$. The 69% increase occurs over a change in α of approximately 0.5°. Then C_D increases more gradually from 0.0821 to 0.2226. This 2.7-fold increase in the drag indicates a progression to total flow separation over the entire flipper at greater α.

The L/D ratio, or aerodynamic efficiency, shows a broad range of operation at a high L/D as shown in Fig. 3(c). This curve characterizes the drag cost of producing lift. The peak occurs at $\alpha = 7.5°$ with a value of $(L/D)_{\max} = 22.5$. This is rather efficient for a section having a 20% thickness.[9] More significantly, the smooth flipper maintains L/D values over 20 through a broad range of incidence angles: $\alpha = 5 - 10°$.

We now shift our focus to the aerodynamic performance measures of the scalloped flipper model that show that the presence of the tubercles delays stall to higher α, increases maximum lift, and decreases drag. For example, below an incidence of approximately 8.5°, the lift curve is largely unchanged from the smooth flipper model results [Fig. 4(a)]. However, the lift curve takes a distinctly shallower slope of $a = 0.494\ \text{deg}^{-1}$ from $\alpha = 8.5° - 14.5°$, yet the trend remains largely linear. Although the C_L for the scalloped model is lower than the C_L for the smooth flipper for a limited range $(9.3 \leqslant \alpha \leqslant 12)$, it is equal to or greater than the results from the smooth model at other angles. We also observe that α_{stall} increases by 40% to 16.3°. Of significant interest and utility is the fact that the value of $C_{L_{\max}}$ increases 6% over the smooth model, from 0.88 to 0.93. Thus, the lift of the scalloped flipper model shows an expanded operating envelope: higher lift at higher incidence angles.

The drag curve for the scalloped flipper, shown in Fig. 4(b), shows pronounced increases with the onset of each aerodynamic state (for example, attached flow, partial stall, and deep stall). At low angles, the drag is no greater than the smooth results. The first break in the lift curve is accompanied by a drag increase of $\Delta C_D = 0.0107$ or 34%, making the drag higher than the smooth results for the limited range of $10.3 < \alpha < 11.8$. Beyond this range, however, the scalloped flipper model produces consistently lower drag than the

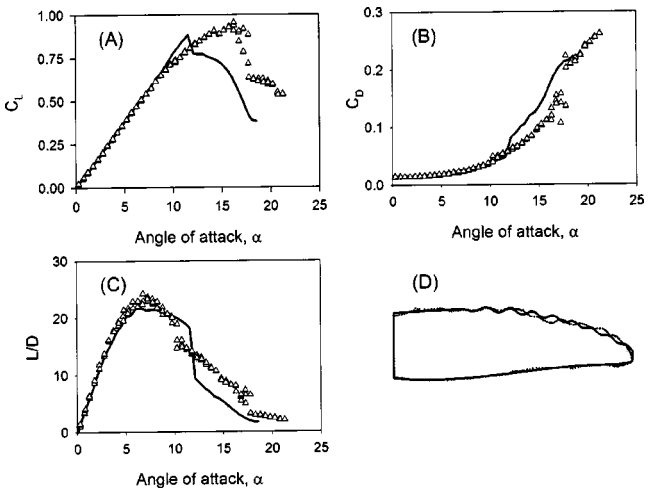

FIG. 4. Lift and drag data for the scalloped whale flipper model. The solid lines in (a), (b), and (c) show, for comparison, the average of the data from the wind tunnel experiments utilizing the smooth flipper model [Figs. 3(a)–3(c)]. (a) Wind tunnel measurement of the lift coefficient, C_L, shown as a function of the angle of attack, α. Note that the scalloped geometry maintains lift to higher angles of attack than the smooth model. (b) Drag coefficient, C_D, shown as a function of the angle of attack. (c) Aerodynamic efficiency, L/D. (d) Profile of the idealized scalloped model (solid line) superimposed on the actual whale flipper profile (dotted line). These measurements show that the scalloped model delays complete stall to $\alpha_{\text{stall}} \approx \pm 17.5°$, a 40% improvement over the stall angle of the smooth model.

smooth model, by as much as 32%. Therefore, the expanded operating envelope is accompanied by a significant reduction in drag, meaning the animal can expend less energy in generating greater maneuvering forces with the flipper.

As a result of the lift and drag characteristics, aerodynamic efficiency is decremented at some incidence angles, but incremented at most others. Figure 4(c) shows L/D for the scalloped geometry. The peak aerodynamic efficiency occurs around the same point as the smooth case ($\alpha = 7.5°$) but has a higher value of 23.2. However, the range of highest values is reduced somewhat: the scalloped model has a lower L/D for $\alpha = 5° - 8.5°$. The L/D ratio is greater at all other incidence angles. This means that the scalloped flipper performs better, proportionately, at most points in the operational envelope, particularly at higher angles.

Our findings, specifically, are that the scalloped leading edge of the flipper serves to delay stall by providing higher lift at higher incidence angles, and to ameliorate the post-stall characteristics by maintaining higher lift with lower drag. The ability to augment performance at high angles of attack would be advantageous for the humpback whale while feeding and maneuvering where an expanded operating envelope is needed. For example, the imbalance in lift between the flippers (high positive lift on one, high negative lift on the other) creates an enhanced ability to roll, and to do so at higher rates.[10] Maximum-lift orientation caused by placing both flippers in the same orientation creates a large pitching moment about the animal's center of mass, enabling the animal to dive or climb quickly. Additionally, a greater imbalance in drag gives the whale added yaw control that allows the whale to turn swiftly. Enhanced maneuvering capabilities permit tighter turns, which give these whales an advantage in their use of "bubble netting" to catch prey.[1,2,6] We should also note that the animal might use "controlled" stall to enhance maneuvering.

From the hydrodynamic performance capabilities of the flippers with the addition of the leading-edge tubercles, we can draw analogies to vortex generators that energize the flow over an aircraft wing. These vortex generators, usually small tabs placed near the leading one-third of the chord of an aircraft wing, cause a greater momentum exchange within the boundary layer than would occur without the vortex generators. This additional momentum transport helps to keep the flow attached to the lifting surface despite an adverse pressure gradient. The dynamics of the vortices serve to maintain or increase lift by preventing stall.[4] The lift-force and drag-force modification created by a scalloped leading edge produce results similar to these produced by vortex generators. Therefore, the enhanced lift and drag effects afforded by a scalloped leading edge offer a possible alternative to tab-like vortex generators for specialized, high-performance lifting surfaces for low Reynolds number autonomous aircraft and for underwater vehicle operation.

This work was supported by the Office of Naval Research (L.E.H. and F.E.F., under separate grants), the Naval Academy Research Council (D.S.M.), and the technical support staff of the United States Naval Academy.

[1] C. M. Jurasz and V. P. Jurasz, "Feeding modes of the humpback whale, *Megaptera novaeangliae*, in southeast Alaska," Sci. Rep. Whale Res. Inst. **31**, 69 (1979).
[2] J. H. W. Hain, G. R. Carter, S. D. Kraus, C. A. Mayo, and H. E. Winn, "Feeding-behavior of the humpback whale, *Megaptera-Novaeangliae*, in the western North-Atlantic," Fish. Bull. NOAA **80**, 259 (1982).
[3] U. M. Norberg, *Vertebrate Flight: Mechanics, Physiology, Morphology, Ecology and Evolution* (Springer-Verlag, Berlin, 1990).
[4] H. D. Taylor, "Summary report on vortex generators," United Aircraft Research Department Report R-05280-9 (1950).
[5] D. M. Bushnell and K. J. Moore, "Drag reduction in nature," Annu. Rev. Fluid Mech. **23**, 65 (1991).
[6] F. E. Fish and J. M. Battle, "Hydrodynamic design of the humpback whale flipper," J. Morphol. **225**, 51 (1995).
[7] D. S. Miklosovic, M. P. Schultz, and C. J. Esquivel, "Effects of surface finish on aerodynamics performance of a representative stabilizer," J. Aircr. (to be published).
[8] J. D. Anderson, *Fundamentals of Aerodynamics Third Edition* (McGraw-Hill, Boston, 2001).
[9] I. H. Abbott and A. E. Von Doenhoff, *Theory of Wing Sections, Including a Summary of Airfoil Data* (Dover, New York, 1959).
[10] D. Weihs, "Stability of aquatic animal locomotion," Cont. Math. **141**, 433 (1993).